Canted Antiferromagnetism in an Organo-modified Layered Nickel Phyllosilicate

Mireille Richard-Plouet,* Serge Vilminot, Murielle Guillot, and Mohamedally Kurmoo

Groupe des Matériaux Inorganiques, Institut de Physique et de Chimie des Matériaux de Strasbourg UMR CNRS−ULP 7504, 23, rue du Loess, 67037 Strasbourg, France

Received February 25, 2002. Revised Manuscript Received June 5, 2002

The hydrothermal reaction of 3-aminopropyltriethoxysilane (APTES) and nickel acetate tetrahydrate at 170 °C results in a layered nickel silicate, $Ni_3Si(C_3H_6NH_3)F_{0.65}O_{1.9}(OH)_{4.45}(CH_3COO)_{1.1}\cdot xH_2O$, $x = 0.38$, with an interlayer spacing of 21 Å. The molecular structure is deduced from powder X-ray diffraction, transmission electron microscopy, X-ray absorption and IR spectroscopies, and a structure is proposed. The structure consists of edge-sharing $Ni(O,OH)_6$ layers separated by aminopropyl silicate and acetate. The magnetic behavior is described by layers of ferromagnetically coupled nickel ions ($C = 1.28$ emu·K·mol^{-1} and $\theta = +35$ K) coupled antiferromagnetically at a Néel temperature of 21 K. A small spontaneous magnetization is observed due to canting of the sublattice magnetizations amounting to 0.7°. Isothermal magnetization measurements at 2 K on oriented samples reveal that the easy axis is perpendicular to the layers and a spin-flop field is observed at 20 kOe.

Introduction

Recently, there has been intense activity in developing layered compounds for various applications, such as catalysis and photocatalysis, for sorption, and for stabilizing emulsions. These applications are due principally to the structural nature of these compounds.[1] Most recently there has been additional interest from magnetochemists due to the realization of long-range magnetic ordering in two dimensions.[2] The kind of materials used to date encompasses the silicates, hydroxides, phosphates, oxalates,[3] etc. The interlayer spacing of these materials can be modified chemically by inserting ions[4,5] or neutral molecules into the galleries, or by connecting organic groups through covalent bonds to the layers. The latter is mostly generated with carboxylates,[6] sulfates[7] or phosphonates,[8] sulfonates,[6b] and amines.[9] Among the silicates this is possible by modifying the silane starting materials. In general, divalent magnesium is used to generate the inorganic layer. The most common synthetic approach is by precipitation from Mg (and in some cases Ni) chloride and an organo-modified alkoxide of silicon with sodium hydroxide in water−alcohol solution. The resulting suspensions are stirred either at room temperature[10−13] or at 50 °C[14−17] or kept under reflux.[18] This procedure leads to relatively poorly crystallized compounds. The crystallinity of these silicates is sufficient to be used for different applications such as in situ intermolecular reactions with guest species[13] or ion adsorption,[19,20] but for the study of their magnetic properties better crystallized materials are preferable. Using a hydrothermal synthetic approach,

* Corresponding author. Telephone: 00 33 388 10 71 29. Fax: 00 33 388 10 72 47. E-mail: richard@ipcms.u-strasbg.fr.

(1) (a) Sato, T.; Yin, S. *Mater. Integr.* **2001**, *14* (2), 39−44. Zhao, H.; Vance, G. F. *Clays Clay Miner.* **1998**, *46* (6), 712−718. (b) Abend, S.; Bonnke, N.; Gutshner, U.; Lagaly, G. *Colloid Polym. Sci.* **1998**, *276*, 730−737.

(2) *Magnetic properties of layered transition metal compounds*; De Jongh, L. J., Ed.; Kluwer Academic Publishers: Dordrecht, 1990.

(3) (a) Nuttall, C.; Day, P. *J. Solid State Chem.* **1999**, *47* (1), 3−10. (b) Bénard, S.; Rivière, E.; Yu, P.; Nakatani, K.; Delouis, J. F. *Chem. Mater.* **2001**, *13*, 159−162.

(4) (a) Atovmyan, L. O.; Shilov, G. V.; Lyuboskaya, R. N.; Zhilyaeva, E. I.; Ovaneyan, N. S.; Pirumova, S. I.; Gusakovskaya, I. G. *JETP Lett.* **1993**, *58*, 766−769. (b) Decurtins, S.; Schmalle, H. W.; Ostwald, H. R.; Linden, A.; Ensling, J.; Gütlich, P.; Hauser, A. *Inorg. Chim. Acta* **1994**, *216*, 65−73. (c) Coradin, T.; Clément, R.; Lacroix, P. G.; Nakatani, K. *Chem. Mater.* **1996**, *8*, 2153−2158.

(5) Gatteschi, D.; Caneschi, A.; Pardi, L.; Sessoli, R. *Science* **1994**, *265* (5175), 1054−1058.

(6) (a) Hornick, C.; Rabu, P.; Drillon, M. *Polyhedron* **2000**, *19* (3), 259−266. (b) Kurmoo, M.; Day, P.; Derory, A.; Estournes, C.; Poinsot, R.; Stead, M. J.; Kepert, C. J. *J. Solid State Chem.* **1999**, *145* (2), 452−459. (c) Kurmoo, M. *Philos. Trans. R. Soc. London, Ser. A* **1999**, *357* (1762), 3041−3061. (d) Kurmoo, M. *Chem. Mater.* **1999**, *11*, 3370−3379.

(7) Laget, V.; Hornick, C.; Rabu, P.; Drillon, M. *J. Mater. Chem.* **1999**, *1*, 169−174.

(8) (a) Fanucci, G. E.; Petruska, M. A.; Meisel, M. W.; Talham, D. R. *J. Solid State Chem.* **1999**, *145* (2), 443−451. (b) Bellitto, C.; Federici, F.; Ibrahim, S. A. *Chem. Mater.* **1998**, *10* (4), 1076−1082.

(9) (a) Mitzi, D. B. *Prog. Inorg. Chem.* **1999**, *48*, 1−121. (b) Rujiwatra, A.; Kepert, C. J.; Claridge, J. B.; Rosseinsky, M. J.; Kumagai, H.; Kurmoo, M. *J. Am. Chem. Soc.* **2001**, *123* (43), 10584−10594.

(10) Fukushima, Y.; Tani, M. *J. Chem. Soc., Chem. Commun.* **1995**, 241−242.

(11) Fukushima, Y.; Tani, M. *Bull. Chem. Soc. Jpn.* **1996**, *69*, 3667−3761.

(12) Burkett, S.; Press, A.; Mann, S. *Chem. Mater.* **1997**, *9*, 1071−1073.

(13) Whilton, N.; Burkett, S.; Mann, S. *J. Mater. Chem.* **1998**, *8* (8), 1927−1932.

(14) da Fonseca, M. G.; Silva, C. R.; Airoldi, C. *Langmuir* **1999**, *15*, 5048−5055.

(15) da Fonseca, M. G.; Airoldi, C. *J. Chem. Soc., Dalton Trans.* **1999**, 3687−3692.

(16) da Fonseca, M. G.; Silva, C. R.; Barone, J. S.; Airoldi, C. *J. Mater. Chem.* **2000**, *10*, 789−795.

(17) Silva, C. R.; da Fonseca, M. G.; Barone, J. S.; Airoldi, C.*Chem. Mater.* Published on the Web Dec 5, 2000.

(18) Carrado, K.; Xu, L.; Csencsits, R.; Muntean, J. *Chem. Mater.* **2001**, *13* (10), 3766−3773.

(19) da Fonseca, M.; Airoldi, C. *Thermochim. Acta* **2000**, *359*, 1−9.

(20) da Fonseca, M.; Airoldi, C. *J. Mater. Chem.* **2000**, *10*, 1457−1463.

10.1021/cm0211498 CCC: $22.00
Published on Web 08/09/2002

we have improved marginally the crystallinity, and here we report the characterization and magnetic properties of a new organo-modified Ni silicate. It is worth noting that previous magnetic studies of the Ni silicate compounds are rare.[21,22]

From a magnetic point of view the layered structured materials are of great interest due to the fact that no long-range magnetic ordering (LRO) is expected for an isotropic Heisenberg system. However, introducing anisotropy through single ion or via spin−orbit coupling may give rise to LRO in low-dimensional materials[23] as in the case of two-dimensional Ising systems. They are of additional interest due to the frustration as a consequence of the triangular arrangement of the moments. To this end, our group is involved in the synthesis of silicates under hydrothermal conditions because of the similarity of the magnetic topology of these silicates to the $M^{II}(OH)_2$ layered compounds.[21,22,24] The transition metal cations are located in brucite-like layers consisting of edge-sharing octahedra with the silicate tetrahedra connected on one or both sides. A schematic figure of the structure has been deposited as Supporting Information. This configuration tends to promote nearest-neighbor ferromagnetic coupling in the case of Ni or Co. In the Ni phyllosilicates LRO occurs at low temperature, presumably through dipolar interaction. Two modifications have been isolated from 3-aminopropyltriethoxysilane. Our first approach in this system led to the characterization of organo-modified clays, corresponding to the following formula: $Ni_3Si_{\approx 2}(C_3H_6NH_3)_{\approx 2}(CH_3COO)_xO_y(OH,F)_z\cdot\approx 2H_2O$. These compounds are constituted of Ni hydroxide type layers to which are grafted the silicate species. Inside the layers, Ni^{2+} ions are coupled ferromagnetically and a ferromagnetic long-range order occurs at a Curie temperature of 18 K, presumably via dipolar interaction. The magnetic behavior is strongly dependent on the Ni-to-Si ratio: when the Ni/Si ratio is 3/2, as in the latter case, the compound is ferromagnetic;[21] when it is 3/1, as in the compound described here, the magnetic ground state is antiferromagnetic. The large difference in magnetic properties between the two derivatives due to a subtle structural change demonstrates the complexity of these systems.

Experimental Section

The new organic inorganic nickel silicate has been synthesized under hydrothermal condition from nickel acetate, 3-aminopropyltriethoxysilane ($RSi(OC_2H_5)_3$, $R = C_3H_6NH_2$), and ammonium fluoride as mineralizing agent. The reactants were set at 170 °C, under autogenous conditions, in a 125 mL autoclave, using a $3Ni/4Si/1NH_4F$ proportion in 50 mL of deionized decarbonated water. Under these conditions the pH is 7.5. The amine is protonated since its pK_a is close to 10. After 2 days, a light green powder was retrieved by centrifugation and rinsed with water. The compound was then dried and stored at 100 °C.

Chemical analyses of 38.85% Ni, 6.45% Si, 2.72% F, 13.77% C, 3.59% H, and 2.98% N suggest a formula $Ni_3Si(C_3H_6NH_3)F_{0.65}O_{1.9}(OH)_{4.45}(CH_3COO)_{1.1}\cdot xH_2O$ ($x = 0.38$), which corresponds to 38.86% Ni, 6.18% Si, 2.72% F, 13.77% C, 3.86% H, and 3.09% N calculated.

The compound was characterized by X-ray powder diffraction (XRD) on a Siemens D5000 diffractometer in a Bragg−Brentano geometry using Cu $K\alpha_1$ radiation ($\lambda = 1.5406$ Å).

Thermogravimetric (TG) and differential thermal (DT) analyses were performed, in air, on a Setaram TGA 92 apparatus, using a heating rate of 6 °C/min.

Electron microscopy was performed on a Topcon 002B microscope operating at a 200 kV accelerating voltage. The sample was prepared by grinding the compound between two glass slides and then collecting it onto a carbon film that has previously been deposited on a copper grid.

Infrared spectra were recorded in transmission mode from powder diluted in a dried KBr pellet, using a ATI Mattson FTIR spectrometer. Raman spectrum was recorded using a Kr laser with a 647.1 nm exciting wavelength.

Oriented films were prepared according to the following conditions. The silicate was dispersed in decarbonated water to obtain a colloidal suspension. Upon settling and slow drying at room temperature, the crystallites were deposited onto Kapton for X-ray absorption, with the layer stacking axis perpendicular to the substrate. For magnetic measurements small free-standing segments were peeled off and aligned in a drinking straw with the applied field perpendicular or parallel to the films.

XAS data at the Ni K edge were recorded on the D42 station of the DCI ring in LURE, at room temperature. The detection of the incident and transmitted beams was performed using air-filled gas ionization chambers. The absorption coefficient was recorded in the 8200−9300 eV range with a 5 eV step scan before the edge, 0.5 eV across, and 2 eV after, using a 2 s accumulating time. Each spectrum was recorded three times and then averaged to increase the signal/noise ratio. The harmonic rejection was performed with a channel-cut (331) Si single crystal monochromator. The $k\chi(k)$ function was extracted from the absorption coefficient using a cubic spline function with the software developed at LURE.[25] E_o was chosen at the very start of the jump, typically between 8378 and 8379 eV. The Fourier transforms were performed on $k^3\chi(k)$ with a Kaiser-Bessel ponderation window ($\tau = 2.5$) in the k-range 2−12 Å^{-1}. As both peaks (three first shells) in the FFT spectrum were well separated (Figure 5), they were fitted independently. We performed a filter on each peak (1−2.1 Å^{-1} for the first peak and 2.1−3.3 Å^{-1} for the second peak). The resulted inverse Fourier transforms were fitted, using FEFF06[26] calculated phase and amplitude corresponding to the different shells around Ni atoms. We used phase and amplitude calculated from $Ni(OH)_2$[27] for Ni−O and from $Ni_3Si_2O_5(OH)_4$[28] for Ni−Ni and for Ni−Si contributions. The validity of these phase and amplitude were checked on the reference compounds before being applied to the sample. For the references, we have fixed the number of neighbors N for each shell and let refine the other parameters of the EXAFS equation:

$$k\chi(k) = -S_o^2\sum_i \frac{N_i}{R_i^2}|f_i(k,R_i)|\exp(-2\sigma_i^2k^2)\exp(-2R_i/\lambda_i(k))\sin(2kR_i + \phi_i(k,R_i))$$

where i is the number of retrodiffusion shell, N_i is the number

(21) Richard-Plouet, M.; Vilminot, S. *J. Mater. Chem*., **1998**, *8* (1), 131−137.

(22) Guillot, M.; Richard-Plouet, M.; Vilminot, S. *J. Mater. Chem.* **2002**, *12* (4), 851−857.

(23) See, for example: *Magnetism: From molecules to materials II*; Miller, J. S., Drillon, M., Eds.;Wiley-VCH: Weinheim, 2001; pp 339−482.

(24) Richard-Plouet, M.; Vilminot, S. *Solid State Sci.* **1999**, *1*, 381−393.

(25) Michalowicz, A. EXAFS pour le Mac, Logiciels pour la Chimie. *Soc. Fr. Chim*. **1991**, 102.

(26) Rehr, J. J.; Mustre de Leon, J.; Zabinsky, S. I.; Albers, R. C. *J. Am. Chem. Soc.* **1991**, *113* (14), 5135−5140.

(27) Crystallographic data obtained from the Rietveld refinement of the powder diffraction pattern of $Ni(OH)_2$ obtained under hydrothermal conditions: $a = 3.13(1)$ Å, $c = 4.61(3)$ Å, $P\bar{3}m1$, Ni: 0 0 0, O, 1/3 2/3 0.244(2).

(28) Hall, S. H.; Guggenheim, S.; Moore, P.; Bailey, S. W. *Can. Mineral.* **1976**, *14*, 314−321.

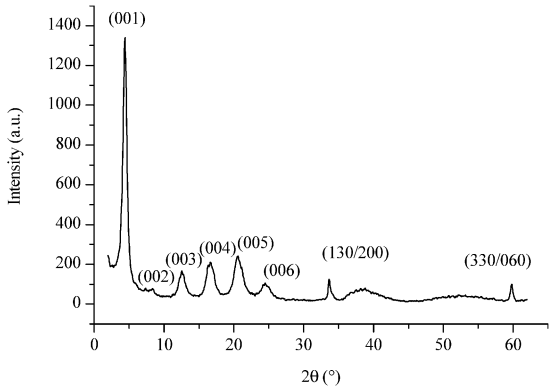

Figure 1. Experimental X-ray diffraction pattern and full pattern matching allowing indexation of the diffraction peaks.

of atoms at a distance R_i from the central Ni atom for each shell, σ_i is the Debye−Waller factor, λ_i is the mean free path, and ϕ_i and f_i are the phase and amplitude for the backscatters i. S_o^2 is the reduction factor (fixed to 1).

For the sample, N_{Si}, σ, and R were obtained by fixing N_O and N_{Ni} equal to 6. The goodness of fit was appreciated through the residual:

$$\rho = \frac{\sum_k (k\chi_{exp} - k\chi_{calc})^2}{\sum_k (k\chi_{exp})^2}$$

Magnetic measurements were performed on a Quantum Design MPMS-XL SQUID magnetometer. Susceptibilities were measured in different applied magnetic fields, ranging from 4 to 500 Oe in the zero-field and field-cooling conditions. Isothermal magnetization measurements versus magnetic field were recorded in fields up to 50 kOe for temperatures ranging from 2 to 21 K. ac susceptibilities from 2 to 25 K were measured in a 3.5 Oe field oscillating at 20 Hz.

Results

The powder X-ray diffraction pattern (Figure 1) is characterized by broad Bragg peaks indicating that the solid is crystallized only on a small scale. Using the most commonly accepted cell choice for 2:1 phyllosilicates ($a \sim 5.3$ Å, $b \sim 9.3$ Å, $c \sim 9.4$ Å, $\beta \sim 100°$),[29] the progression of diffraction peaks at low θ can be indexed as (00l), whereas the narrow peaks at 2.680(3) and 1.553(2) Å are indexed as (130, 200) and (060, 330), respectively. From the width of the peaks and using the Scherrer formula,[30] the diffraction coherence length was evaluated to 8 nm in the [001] direction and 25 nm transversely. By comparison with nickel hydroxide and phyllosilicates or organo-modified metal silicate diffraction patterns, it can be assumed that Ni^{2+} ions in the present compound are arranged in the same way. The occurrence of (hk) peaks at 2.680(3) Å and 1.553(2) Å strongly suggests that the Ni^{2+} ions are disposed as in brucite, forming a two-dimensional triangular array. However, the quality of the diffraction pattern does not allow for the determination of the atomic coordinates. It must be noticed that the hydrothermal treatment marginally enhances the crystallinity of the phase obtained compared to precipitation methods. Moreover, our compound has an interlayer distance of 20.7 Å, which is longer than the one obtained by other authors using the same alkoxide: 18.5 Å with Mg,[13] under neutral condition, and 16.4 Å starting from Ni nitrate,[16] at pH 12. The difference is due to the presence of acetate in the place of chlorine for Mg silicate. In the Ni nitrate case, the pH condition probably leads to the incorporation of the amino group as RNH_2 and no counteranion is necessary.

From transmission electron microscopy, the interlayer distance was also measured from high magnification images. It is noticed that only a few layers are coherently stacked (Figure 2a), which is responsible for the X-ray diffraction peaks broadening. The electron diffraction pattern (Figure 2b) performed on platelets is characteristic of a [001] zone axis powder-like diagram with two intense rings at 2.68(9) and 1.55(3) and one diffuse at 1.34(3) Å. The corresponding indexing is shown in Figure 2c.[31] We have also checked by energy-dispersive X-ray spectroscopy the chemical homogeneity of the sample. None of the crystallites appear to be organosilica or $Ni(OH)_2$, which may have precipitated during the synthesis.

From the IR spectrum presented in Figure 3 some characteristic features can be distinguished: for instance, the occurrence of a sharp peak at 3630 cm^{-1} corresponding to the stretching vibration of free O−H hydroxyl groups, bands corresponding to the propylammonium (at 3300, 3086, 2100, and 1640 cm^{-1}). The presence of acetate ions is evidenced through the ν_{as} and ν_s vibrations at 1560 and 1412 cm^{-1}, respectively. The band at 1190 cm^{-1} is attributed to the Si−C vibration, confirming that the hydrothermal treatment does not affect the alkoxide. Finally, a broad band at 990 cm^{-1} with shoulders at 1086 and 1051 cm^{-1} is attributed to the Si−O skeleton. Acetates and amines are better distinguishable by Raman spectroscopy by bands appearing at 648, 917, and 1414 cm^{-1} for acetates[32,33] and 1647 cm^{-1} attributed to NH_3^+, i.e., protonated amine. This protonation is also evidenced through the weak band at 2100 cm^{-1} on IR spectrum. This result was also observed for Mg modified silicates obtained from 3-aminopropyltriethoxysilane[12] or 3-(2-aminoethyl-3-aminopropyl)trimethoxysilane[13] with Cl^- as counteranion. The possibility to exchange the acetate group has been explored by stirring a suspension of the silicate in an aqueous solution of Cu phthalocyaninetetrasulfonic acid tetrasodium salt. The change in coloration from light green to deep blue, after thorough washing and the observation of a d_{001} peak shift toward 25.3 Å, indicates that the interlayered space can be tuned via ionic exchange. In addition, in the IR spectrum, the acetate bands disappear and are replaced by bands characteristic of the Cu complex, especially those of the sulfonate vibrations.

Within the unit cell assumed above and for $Z = 2$, the following formula unit can be proposed: $Ni_3Si(C_3H_6NH_3)F_{0.65}O_{1.9}(OH)_{4.45}(CH_3COO)_{1.1}\cdot xH_2O$, $x = 0.38$. This formula is based on the chemical analyses that are given

(29) Bailey, S. W. *Reviews in mineralogy, Hydrous phyllosilicates*, Proceedings of the Mineralogy Society of America, Chelsea, MI, 1991; Wiley Interscience: New York, 1991, Vol. 19.
(30) Scherrer, P. *Gött. Nachr.* **1918**, *2*, 98.
(31) Morniroli, J. P.; Winter, L.; Vankeiken, D. Electron Diffraction, software version 3.8, 1999.
(32) Frost, R. L.; Tran, T. H.; Kristof, S. *Vib. Spectrosc.* **1997**, *13*, 175−186.
(33) Frantz, J. D.*Chem. Geol.* **2000**, *164*, 1−20.

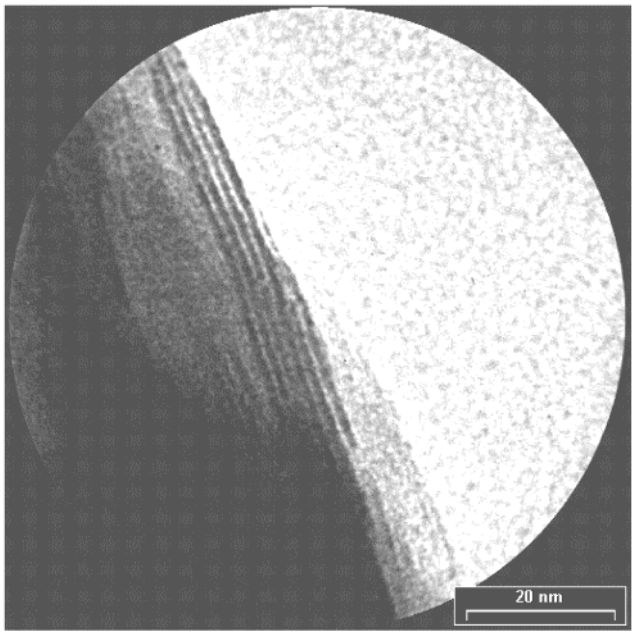

Figure 2. (a) Transmission electron microscopic image revealing the low coherent stacking of the layers. (b) Electron diffraction performed on an oriented hybrid silicate. (c) [001] zone axis simulation obtained from a monoclinic cell in which brucite layers are separated by 21 Å.

in the Experimental Section. The water content is not easy to evaluate because it is strongly dependent on the

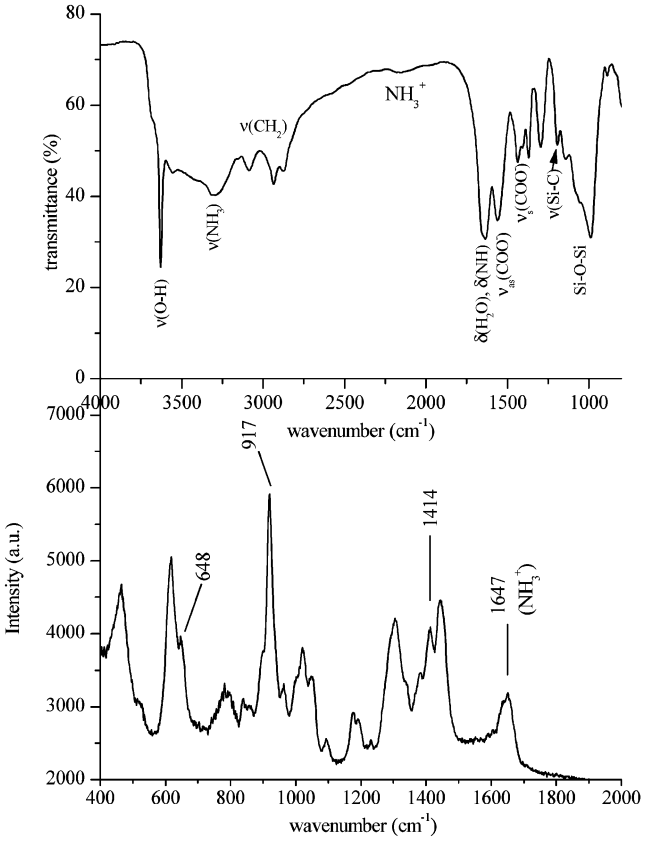

Figure 3. IR and Raman spectra performed on powder sample.

storage conditions of the powder. Thermogravimetric analysis reveals that the first weight loss (−1.5%) taking place at low temperature (<120 °C) can be attributed to the removal of water, mainly adsorbed at the surface of the grains. The presence of water is seen by a broad band in the 3500−3000 cm^{-1} range in the IR spectrum. It is important to note that this stoichiometry is obtained only in an excess of APTES. The low content of Si in the solid, compared to the 3Ni/4Si initial proportion, is attributed to the formation of small oligomers that remain soluble in the filtrate. Attempts to obtain this silicate from a stoichiometric ratio (Ni/Si = 3) leads mainly to the precipitation of $Ni(OH)_2$. It seems that a large excess of initial Si alkoxide is necessary in order to transfer the equilibrium toward the silicate formation. Oxygen and hydroxide proportions are determined from charge balance and the number of available anionic sites on the layer.

From TGA curves, the weight loss is in agreement with the one deduced from the chemical analysis, 37.3% versus 36.6%. The decomposition under air is characterized by several exothermic peaks between 250 and 450 °C, corresponding to the combustion of the organic species (acetate and aminopropyl group), leading to a NiO and SiO_2 mixture.

The Fourier transform of the EXAFS oscillations presents two main peaks (Figure 4). The first one at 1.6 Å (not corrected for phase shift) can be attributed to the first coordination sphere of Ni, which is six oxygen atoms in an octahedral coordination. Subsequent fitting of the inverse Fourier transform of this peak with theoretical phase and amplitude calculated for $Ni(OH)_2$

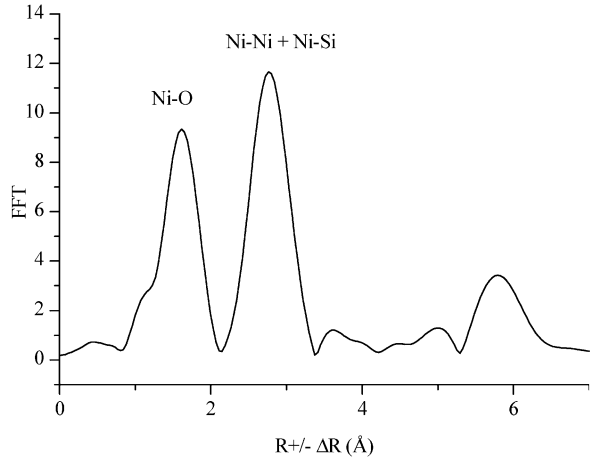

Figure 4. Fourier transform of the EXAFS signal, performed on $k^3\chi$.

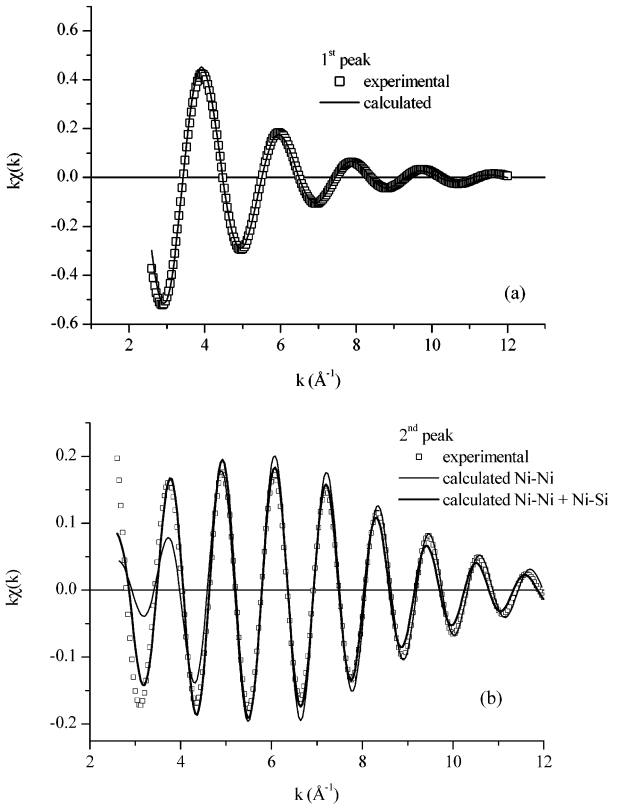

Figure 5. (a) Inverse Fourier transform performed on the first peak, corresponding to the first coordination sphere around Ni and fit of the oscillations with six oxygens at 2.05 Å. (b) Inverse Fourier transform performed on the second peak, corresponding to the second and third coordination spheres around Ni and fit of the oscillations with either 6 Ni at 3.10 Å (Ni−Ni) or 5.9 Ni at 3.10 and 1.7 Si at 3.27 Å (Ni−Ni + Ni−Si).

leads to six oxygen atoms at 2.05(2) Å, with $\sigma = 0.087$ and $\rho = 0.4\%$ (Figure 5a). For the second peak, fitting has been performed by considering either only Ni in the second coordination sphere ($Ni(OH)_2$ phase and amplitude) or a combination of Ni and Si ($Ni_3Si_2O_5(OH)_4$ phase and amplitude). As shown in Figure 5b, the best fit is observed in the second case for 5.9(1.1) Ni at 3.10-(2) Å, $\sigma = 0.092$, and 1.7(3) Si at 3.27(2) Å, $\sigma = 0.094$, $\rho = 4\%$. The discrepancy in the Si content is due to the low electron density of Si compared to Ni. We can therefore conclude that the silicate species are grafted

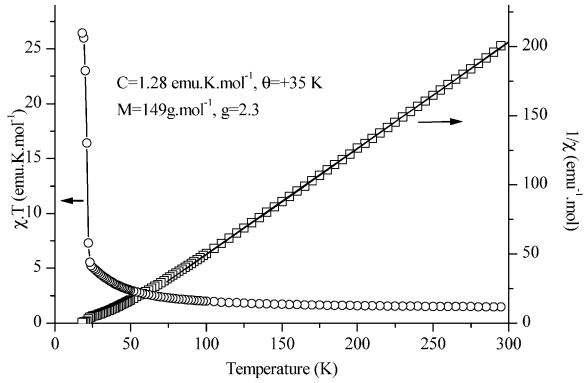

Figure 6. Inverse of the susceptibility and χT versus temperature, performed with a 100 Oe applied field on the powder silicate.

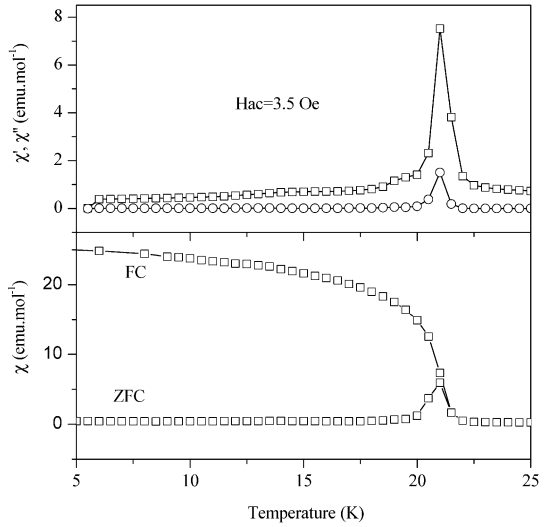

Figure 7. Alternative susceptibility (3.5 Oe, 20 Hz) (top); FC, ZFC susceptibilities under 4 Oe (bottom).

to the nickel layers via Ni−O−Si covalent bonds and the presence of acetate in the gallery is in agreement with an estimated interlayer distance close to 21 Å.

The temperature dependence of the dc susceptibility is depicted in Figure 6 for $1/\chi$ and χT, performed in an applied field of 100 Oe. The data can be fitted to the Curie−Weiss law ($\chi = C/(T - \theta)$) in the 100−295 K temperature range with $C = 1.28$ emu·K·mol^{-1}, $\theta = +35$ K. The results indicate that nearest-neighbor ferromagnetic interaction is dominant at high temperature as also seen by the increase of the χT product at low temperature. The Landé factor, $g = 2.3$, deduced from the spin-only equation (Curie constant $= Ng^2\mu_B{}^2S(S + 1)/3k$, $S = 1$) is in agreement with the expected value for Ni^{2+} in octahedral coordination. The normal range of the value of the Curie constant confirms indirectly the molar mass per Ni^{2+} found from chemical analysis: 149 g·mol^{-1}. Upon cooling spontaneous magnetization is observed at 21 K. This transition is characterized by very sharp peaks in the χ' and χ'' components of the ac susceptibilities (Figure 7, top).

We note that the peaks in the ac susceptibilities are at the same temperature that indicates a low dimensionality of the magnetism. Zero-field-cooling (ZFC)−field-cooling (FC) susceptibilities in a low applied field of 4 Oe are shown in Figure 7, bottom. A bifurcation point is observed at 21 K. At 2 K, the magnetization

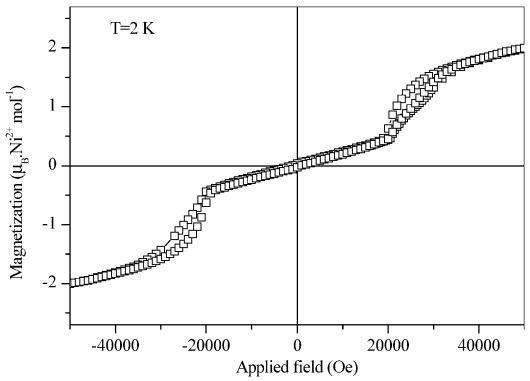

Figure 8. Magnetization versus applied field at 2 K recorded for a powder sample.

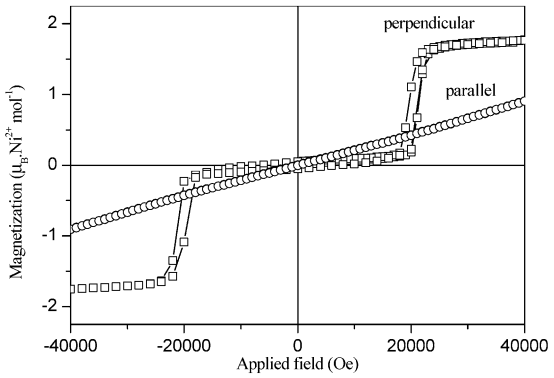

Figure 9. Magnetization versus applied field at 2 K performed on an oriented silicate with the applied field perpendicular and parallel to the film.

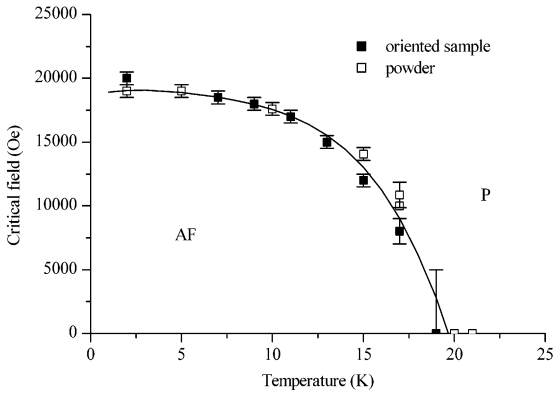

Figure 10. Dependence of the spin-flop critical field upon temperature.

versus field curve, depicted in Figure 8, is not characteristic of a ferro- or ferrimagnetically ordered material. First, we note a strong dependence on the orientation of the sample (Figure 9). Measurements made on a polycrystalline sample show a linear dependence of magnetization with field up to 20 kOe, followed by a sharp increase. The magnetization then increases gradually to 50 kOe. The value of the magnetization at 50 kOe is quite close to the fully aligned moment expected for Ni^{2+} (2 μ_B). From temperature dependence of the critical field, we constructed the phase diagram shown in Figure 10. The critical field is obtained by the first inflection point on the magnetization curve (numerical derivative). This behavior pertains to those of antiferromagnets. The spontaneous magnetization is therefore due to a small canting. The nature of the H_c temperature dependence suggests that the field-induced transition corresponds to a spin-flop. Measurements on an aligned sample (Figure 9) reveal that the easy axis is perpendicular to the layers. Several samples with variable water quantity were measured; no influence of this parameter on the magnetic behavior was brought to the fore.

On close inspection of the isothermal magnetization at 2 K (Figure 9), we found there is a very small hysteresis at the spin-flop transition and a very wide hysteresis and small remanence are observed around zero field, possibly related to the small canting. The hysteresis width at the spin-flop is 1600 Oe. The coercive field for the loop around zero field is surprisingly high (6800 Oe), and the remnant magnetization is 0.050 $\mu_B \cdot mol^{-1}$. The estimated canting angle is 0.7°. This angle is calculated according to the equation arcsin($M_{rem}/2M_{sat}$), where M_{rem} is the remanant magnetization at 2 K and M_{sat} is the expected saturation magnetization if all the moments are aligned ferromagnetically. The coercitive field measured on a powder sample is close to 1000 Oe, which is lower than the value obtained when the applied field is along the easy axis.

To compare this silicate with the previously reported one, their characteristics are summarized in Table 1. From the structural point of view, the two phases exhibit similar chemical features: protonation of the amino group, presence of acetate as counteranion, interlayer distance close to 21 Å, grafting of the silicate species to the brucite-like sheets. The differences reside in the improved quality of the X-ray diffraction pattern for the present silicate and the lower Si content. At high temperature, in the paramagnetic region, the two compounds present ferromagnetic interactions with similar θ values. The latter is in good agreement with that expected for similar arrangement of the moment carriers within the layer. Another difference is in the low-temperature magnetic ground state. The occurrence of an antiferromagnetic ground state in the present compound compared to a ferromagnetic one observed previously is due to the difference in the sign of the interlayer exchange interaction. The possibility of a greater disorder, due to a higher amount of silicate species, in the interlayered space in the already published compounds, may alter the magnetic exchange pathway between layers.

Discussion

The present nickel silicate is built up from Ni hydroxide type layers with grafted silicate species. The aminopropyl group bound to Si and the acetate in the gallery lead to a 21 Å interlayer spacing. Using the thickness of the inorganic part as found for the 2:1 phyllosilicate (ca. 9.4 Å) and assuming the organic species are perpendicular to the layer (twice 5 Å for the propylamine) give 19.4 Å, in agreement with that found in ref 14. The presence of acetate, evidenced by IR and Raman spectroscopies, and chemical analysis results in an interlayer distance close to 21 Å (Figure 11). We believe the acetate forms an ion pair with the ammonium since the ratio of the two is close to unity. Consequently, the acetate would lie perpendicular to the inorganic layer, adding to the spacing. From a chemical point of view, under the hydrothermal synthesis we

Table 1. Main Characteristics of the Two Nickel Silicates with Aminopropylsilane[a]

Ni/Si	θ (K)	C (emu·K·mol^{-1})	$T_{transition}$ (K)	d_{001} (Å)	magn ground state at low temp
3/2[21]	+31 (1)	1.15	15	21	ferromagnetic
3/1 (this work)	+35 (1)	1.28	21	20.7	canted antiferromagnetic

[a] Obtained at neutral pH.

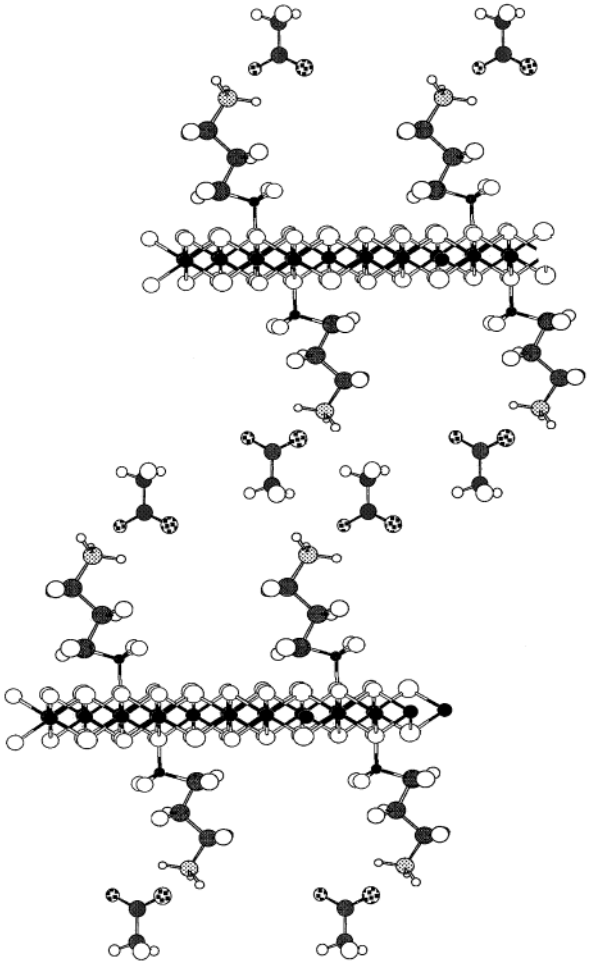

Figure 11. Schematic representation of the organo-modified Ni phyllosilicate with Ni/Si = 3/1.

cannot assume a hexagonal arrangement of Si tetrahedra as in 2:1 phyllosilicates since this geometry is no longer possible due to the Si−C bond which prevents sharing of the apexes of neighboring tetrahedra as in clay structures. The presence of a large organic group also results in the packing of less silicon to the nickel layer. We should note that the stability of the structure does not depend on the complete condensation of the silicate as in 2:1 phyllosilicate. This stability is evidenced by a high-temperature decomposition of 400 °C. Although the presence of interlayer Ni^{2+} has been previously proposed for these materials, there is no clear evidence in our structural and magnetic results to justify these claims.

As evidenced by the positive θ value, ferromagnetic interaction dominates at high temperature. Since the structure is built up of Ni hydroxide layers, the intralayer exchange interaction is expected to be ferromagnetic. Ferromagnetically coupled layered compounds are also known in the diphosphonate $Ni_4(O_3P(CH_2)PO_3)_2 \cdot (H_2O)_n$.[34] According to recent works based on Cu and Co hydroxide type materials, dipolar interaction can become preponderant in the establishment of low-temperature magnetic ordering.[35] In this case, the direction of the magnetic moments with respect to the layers precluded the sign of the interaction and thus the transition toward a ferromagnetic or an antiferromagnetic order. Thus, dipolar interaction can induce a ferromagnetic ordering when the moments are perpendicular to the layers, whereas the transition toward an antiferromagnetic state can occur when the moments are parallel to the layers. Our experiment on an oriented sample confirms that the easy axis is perpendicular to the layers. However, at low temperature, an antiferromagnetic state is stabilized. Therefore, we can only conclude that in this case dipolar interaction, if present, is negligible and that the long-range antiferromagnetic ordered ground state, at low temperature, is due to antiferromagnetic exchange between nearest-neighbor layers. One possible mechanism is that the exchange between layers is promoted by hydrogen bonds between the organic moiety. This feature would be similar to the situation described in $Ni(OH)_2$ in which Ni^{2+} next nearest neighbors are coupled ferromagnetically leading to "ferromagnetic layers" with the moments perpendicular to the layers. At low temperature they order antiferromagnetically by exchange occurring through hydrogen bonds of the hydroxide.[36]

However, we found a spontaneous magnetization at T_N due to possibly a small canting of the moments in the sublattices. The canting angle is estimated to be 0.7°, which is much larger than those found for layered manganous compounds[37] and less than those found for ferrous compounds.[38] This is in good agreement with a medium anisotropy for nickel. Classical canted antiferromagnetism is observed in systems where two magnetic sublattices exist with antiferromagnetic interactions between them. The noncollinearity of the moment direction induces the canting.[39] In the present case, the canting may be due to the noncollinearity of the moments from one layer to the other. The canting also results in a multidomain state at 2 K after zero-field cooling since the magnetization in zero field is negligible. It also leads to a hysteresis loop with a large coercivity. The origin of this large coercivity is not clear presently, but may be a consequence of the perpendicular alignment of the moment and the small particles. The large coercivity can also come from contribution through dipolar interactions.

(34) Gao, Q.; Guillou, N.; Nogues, M.; Cheetham, A. K.; Ferey, G. *Chem. Mater.* **1999**, *11*, 2937−2947.

(35) (a) Panissod, P.; Drillon, M. *From molecules to materials IV*; Miller, J. S., Drillon, M., Eds.; Wiley-VCH: Weinheim, 2002. (b) Drillon, M.; Panissod, P.; Rabu, P.; Souletie, J.; Ksenofontov, V.; Gütlich, P. *Phys. Rev. B* **2002**, *65*, 104404-1−104404-8.

(36) Suzuki, M.; Suzuki, I. S.; Enoki, T. *J. Phys.: Condens. Matter* **2000**, *12*, 1377−1397.

(37) Fanucci, G. E.; Krzystek, J.; Meisel, M. W.; Brunel, L. C.; Talham, D. R. *J. Am. Chem. Soc.* **1998**, *120*, 5469−5479.

(38) Kurmoo, M.; Kepert, C. J. *New J. Chem.* **1998**, *22* (12), 1515−1524.

(39) Gutschke, S. O. H.; Price; D. J.; Powell, A. K.; Wood, P. T. *Angew. Chem., Int. Ed.* **1999**, *38* (8), 1088−1090.

Conclusion

A organo-modified Ni phyllosilicate has been synthesized by hydrothermal technique and characterized by different methods. The structure is proposed to consist of Ni hydroxide like layers of Ni separated by an organosilicate and acetate. The magnetism is derived from antiferromagnetically coupled ferromagnetic layers, with a canting (0.7°) resulting in a spontaneous magnetization. The spin-flop field is 20 kOe.

Acknowledgment. Dr. Agnès Traverse (LURE, Orsay) is thanked for recording and help in analysis of the XAS spectra, and Dr. Jean-François Bardeau (LPEC, Le Mans) is thanked for the Raman spectroscopy.

Supporting Information Available: Figure 1 giving a representation of phyllosilicate 2:1 structure in the (*b*,*c*)-plane (PDF). This material is available free of charge via the Internet at http://pubs.acs.org.

CM0211498